

THE NATURE OF BLUE EARLY-TYPE GALAXIES IN THE GOODS FIELDS

Joon Hyeop Lee, Myung Gyoon Lee, and Ho Seong Hwang

Astronomy Department, School of Physics and Astronomy, FPRD, Seoul National University, Seoul 151-742, Korea

jhlee@astro.snu.ac.kr, mglee@astrog.snu.ac.kr, hshwang@astro.snu.ac.kr

ABSTRACT

We present a study of the nature of the blue early-type galaxies (BEGs) in the GOODS north and south fields using the GOODS HST/ACS archival data. Using visual inspection, we have selected 58 BEGs and 113 normal red early-type galaxies (REGs) in the sample of 1,949 galaxies with spectroscopic redshifts. We find that the BEGs are generally bluer, fainter, and less-massive than the REGs, although a few BEGs are exceptionally bright and massive. The number fraction of the BEGs to total early-type galaxies is almost constant (~ 0.3) at $z \leq 1.1$. In addition, we find that the size of the BEGs in given redshift bin decrease as redshift decreases. The BEGs look similar to the REGs in the images and surface brightness profiles. However, at least 27 BEGs show traces of tidal disturbances in their fine structures: elongated cores, off-centered cores, asymmetric internal color distributions, tidally distorted outer structures, collisional rings, or very nearby companions. Twenty-one BEGs are detected in the X-ray bands and eleven of them are as luminous as $L_{0.5-10\text{keV}} \geq 10^{43.5} \text{ erg s}^{-1}$, indicating the existence of AGNs in their centers. These results show that at least a half of the BEGs may be descendants of mergers/interacting-galaxies and that at least a quarter of the BEGs may be AGN-host galaxies. The BEGs may evolve into REGs, and the size evolution of the BEGs is consistent with the galactic *downsizing* scenario.

Subject headings: cosmology: observations — galaxies: elliptical and lenticular, cD — galaxies: evolution — galaxies: formation — galaxies: structure

1. INTRODUCTION

Early-type galaxies are one of the key objects in the modern observational cosmology. One of the fundamental questions about early-type galaxies is their formation history, which is closely related to the history of cosmic mass assembly and cosmic star-formation (Lee 2003). There are two competing models for the formation of massive elliptical galaxies. One is a monolithic collapse model, according to which massive elliptical galaxies were formed via a single collapse of proto-galactic cloud followed by a rapid formation of stars (Partridge & Peebles 1967; Tinsley 1972; Larson 1974). The other is a hierarchical merging model where massive galaxies were

formed through continuous merging and accretion of smaller galaxies (Toomre 1977; Searle & Zinn 1978).

The properties of early-type galaxies at low redshift are relatively well known in many aspects thanks to a tremendous number of studies for several decades: the surface brightness profiles of early-type galaxies follow the $R^{1/4}$ law (De Vaucouleurs 1948); there is a strong correlation between luminosity and central velocity dispersion of early-type galaxies (Faber & Jackson 1976); early-type galaxies show very slow rotation (Bertola & Capaccioli 1975; Illingworth 1977; Davis et al. 1983); there are poor cold-gas contents in early-type galaxies, implying rare star-formation events (Faber & Gallagher 1976); the color and magni-

tude of early-type galaxies are strongly correlated (Visvanathan & Sandage 1977); there is a tight correlation among size, surface brightness, and velocity dispersion of early-type galaxies (fundamental plane; Lucey et al. 1991; Jørgensen et al. 1993); and the center of an early-type galaxy is redder than its outer part (Vigroux et al. 1988; Franx et al. 1989). However, it is still unclear whether all early-type galaxies have such ‘typical’ properties. Because understanding the property variation of early-type galaxies along redshift makes it possible to constrain the model for the evolution of early-type galaxies more strongly, it is needed to observe and investigate early-type galaxies in the deep universe.

Recent studies based on the HST images found a new class of early-type galaxies in the distant universe that have different properties from nearby early-type galaxies. Abraham et al. (1999) showed from the analysis of internal color dispersion that 40% of early-type galaxies (four out of eleven) at $0.4 < z < 1$ in the Hubble Deep Field (hereafter HDF; Williams et al. 1996) have evidence of current star-formation. Menanteau et al. (1999) also identified three star-forming E/S0 galaxies among the HDF galaxies. Subsequently, Menanteau et al. (2001a) estimated the surface color dispersion of the HDF objects and reported that about 30% of 79 spheroidals show strong internal-color variation, indicating the existence of not only old stellar populations but also young stellar populations. These objects generally show a bluer center than its outer part, unlike typical nearby early-type galaxies. Menanteau et al. (2001b) tried to explain the origin of the blue centers with a multi-zone single-collapse model, in which late infalls of material into the high-potential core could cause prolonged star-formation in the central region of a galaxy. Blue E/S0 galaxies were also found in other HST fields. Im et al. (2001) found ten blue spheroids at $0.2 < z < 1$ from the HST ‘Groth Strip’ (Groth et al. 1994) data. Based on the small velocity dispersions of those spheroids, Im et al. (2001) concluded that they are low-mass systems suffering late star-formation events. Later, Menanteau et al. (2004) identified early-type systems with inhomologous internal colors (30%–40% of 116 spheroids) in the HST/ACS UGC 10214 field using photometric redshifts. They suggested that the internal color distribution of these objects

can be explained by recent star-formations, and that the fraction of ‘active systems’ does not vary severely at $z < 1$. In addition, Menanteau et al. (2005) pointed out in a study of early-type galaxies in Abell 1689 that the existence of an AGN in a galaxy is another possible origin of the blue center in these galaxies.

Blue E/S0 galaxies were also found in two recent great missions: UDF (Hubble Ultra Deep Field; Beckwith et al. 2003) and GOODS (Great Observatories Origins Deep Survey; Dickinson et al. 2003). Elmegreen et al. (2005a) found 30 early-type galaxies with blue central clumps in the UDF, and estimated the sizes, masses, and ages of six galaxies with spectroscopic redshifts. They found that the six galaxies are 1 – 5 Gyr old (and their clumps are younger than 100 Myr) and a half of them are more massive than $10^{10} M_{\odot}$, although there could be some degeneracy and model-dependence in those estimations. Ferreras et al. (2005) analyzed the statistical properties of 249 early-type galaxies in the southern GOODS field, and reported that one third of the early-type galaxies at intermediate redshifts have blue colors. Based on the analysis of the color gradients, color scatters, and redshift-variations, they concluded that there exist a clear cut between blue E/S0 galaxies and red E/S0 galaxies in their color, and that the ‘two-burst formation scenario’ can reproduce the blue E/S0 galaxies. However, fine structures of these blue galaxies were rarely investigated in previous studies.

In this paper, we present a study of the nature of the blue early-type galaxies in the GOODS north and south fields, based on the GOODS HST/ACS archival data. We use only galaxies with spectroscopic redshift and focus on studying the fine structures of the target galaxies. The outline of this paper is as follows. Section 2 describes the data set we used, and §3 explains our selection process for blue early-type galaxies. We present the results of our photometric, structural, and statistical analyses of the blue early-type galaxies in §4. Primary results are discussed in §5, and a summary and conclusions are given in §6. Throughout this paper, we adopted the cosmological parameters: $h = 0.7$, $\Omega_{\Lambda} = 0.7$, and $\Omega_M = 0.3$.

2. THE DATA

The GOODS is a survey project to observe deep and wide universe with the most powerful facilities covering a large range of wavelength. As a part of the GOODS program, the HST Treasury program was carried out to obtain deep optical images of two fields (the Hubble Deep Field North (HDFN) and the Chandra Deep South (CDFS)) with four filters: F435W(B), F606W(V), F775W(i), and F850LP(z). The total exposure times are 7,200, 5,000, 5,000, and 10,660 seconds for B , V , i , and z , respectively, and the total spatial coverage is about 300 square-arcminutes. The pixel scale of the released drizzled-images is 0.03 arcsec per pixel, and the average PSF FWHM is about 0.1 arcsec. We used the GOODS HST/ACS images and photometry catalogs (version 1.1) publicly released on 2004 April 9 (Giavalisco et al. 2004). Among the objects in the photometric catalogs, we selected galaxies whose spectroscopic redshifts are available in the literature (Cohen et al. 2000; Cristiani et al. 2000; Croom et al. 2001; Dawson et al. 2001; Bunker et al. 2003; Steidel et al. 2003; Cowie et al. 2004; Dickinson et al. 2004; Le Fèvre et al. 2004; Stanway et al. 2004a,b; Strogler et al. 2004; Szokoly et al. 2004; van der Wel et al. 2004; Vanzella et al. 2005)¹: 1,017 galaxies in the HDFN and 932 galaxies in the CDFS (1,949 galaxies in total). For the CDFS galaxies, their spectra in the *GIF* format were retrieved from the web-site² provided by *ESO Astrophysical Virtual Observatory*, and were used for inspecting spectral line features. In addition, we used the X-ray data in two *Chandra* observational catalogs (Giacconi et al. 2002; Alexander et al. 2003) for the selected galaxies. We matched optical objects with X-ray sources within 0.5 arcsec positional tolerance that is almost the same as the pixel scale of *Chandra* images.

3. SAMPLE SELECTION

3.1. Selection of Early-type Galaxies

From the data set of 1,949 galaxies with spectroscopic redshifts, we selected early-type galax-

ies by visual inspection of the images. Because these GOODS galaxies are at various redshifts from $z \approx 0$ to $z \approx 5$, the rest-frame wavelength of one galaxy at given redshift can be largely different from that of another galaxy at different redshift in the same band. To avoid the selection effect that can be caused by the morphology dependence on wavelength, we inspected all four band images of each galaxy considering its rest-frame wavelength, according to the following steps.

First, we set five redshift bins: 0 – 0.087, 0.087 – 0.515, 0.515 – 0.938, 0.938 – 1.125, and beyond 1.125. Each redshift bin is set so that a range in which the rest-frame central wavelength of each band (B , V , i , and z) is not shorter than 4,000 Å break at which a sudden spectral break occurs due to old stellar populations. For example, the rest-frame central wavelength of the B_{435} band at $z = 0.087$ is exactly 4,000 Å and the rest-frame central wavelength of the V_{606} band at $z = 0.515$ is also 4,000 Å. Therefore, in the redshift range from 0.087 to 0.515, the V , i , and z bands show rest-frame optical images but the B band shows images of $\lambda_0 < 4,000$ Å. After setting the redshift bins, we conducted visual classification using all four band images for each object. We considered as early-type galaxies those which look circular or elliptical, but with little hint of disk in the bands of $\lambda_0 \geq 4,000$ Å. Since rest-frame optical images at $z > 1.125$ in any GOODS band were not available, we classified as early-type those galaxies that have circular or elliptical morphology in the z band.

We repeated this procedure three times and determined the final classes with the median of the three independent classification results. The number of galaxies finally classified as early-type is 171. We compared our classification to that of Bundy et al. (2005) who classified galaxies visually in the same fields. It is found that 88% of our early-type galaxies were classified as E, E/S0, compact galaxy, or star by Bundy et al. (2005), but only 62% of the objects that ranked as E, E/S0, compact galaxy, or star by Bundy et al. (2005) are classified as early-type in our study. Three objects in our sample of early-type galaxies classified as stars by Bundy et al. (2005) are not stars but probably compact galaxies, because they have spectroscopic redshifts larger than 0.3. This comparison shows that the classifications in the two studies are consistent, but that our sam-

¹The master compilation of GOODS/CDFS spectroscopy is available at http://www.eso.org/science/goods/spectroscopy/CDFS_Mastercat/

²http://archive.eso.org/wdb/wdb/vo/goods_CDFS_master/form

ple was selected more strictly. The small disagreement is partially due to the different criterion for the UV images at the rest-frame wavelength.

Because we selected early-type galaxies in a sample combined from various redshift surveys, our sample is heterogeneous. The number of redshift surveys referred here is fifteen, and a major fraction of redshift data at $z < 2$ were retrieved from five surveys (Cohen et al. 2000; Cowie et al. 2004; Le Fèvre et al. 2004; Szokoly et al. 2004; Vanzella et al. 2005). These five surveys have slightly different flux limits in selecting spectroscopic targets: $R = 24$ in Cohen et al. (2000), $R = 24.5$ in Cowie et al. (2004), $I = 24$ in Le Fèvre et al. (2004), $R = 26$ in Szokoly et al. (2004), and $z = 24.5$ in Vanzella et al. (2005). In four redshift surveys except Vanzella et al. (2005), targets were selected with nearly unbiased methods (basically magnitude limited). In the sample of Vanzella et al. (2005), main targets were selected among the galaxies with $(i - z) > 0.45$, which may be somewhat biased to red galaxies (possibly early-type galaxies). Nevertheless, our sample is still useful in probing the nature of blue early-type galaxies.

We discuss a possible bias in using only-spectroscopic sample. Even if a target selection itself in a spectroscopic survey is not biased, it is plausible that the success rate in securing spectra is higher in objects with strong lines than in objects with weak lines. This can result in the excess of the late-type ratio in the whole sample, or in the case of our study, the excess of the blue-early-type ratio in the early-type sample (if we suppose that the blue early-type galaxies have typically stronger lines than the red early-type galaxies). This is an unavoidable effect as long as we use spectroscopic sample. Photometric redshifts could be used as well, but current estimates of the photometric redshifts of the galaxies in the GOODS fields are not perfect. In particular it is not easy to derive a reliable estimate of the redshift for blue early-type galaxies that are main targets in this study. We decided to use only the spectroscopic redshifts because we needed accurate values of the redshifts for the target galaxies.

The fraction of the early-type galaxies in our sample is 9% (=171/1949). This is somewhat smaller than the result of Bundy et al. (2005) who classified the galaxies visually using the same images of the GOODS field, obtaining 14% (E,

E/S0 in their sample). Our result is similar to the results of Elmegreen et al. (2005b) who classified the galaxies visually using the HST/ACS images of the UDF, obtaining 11%. However, it is smaller than those based on the automatic classification: Conselice et al. (2005) obtained 20–30% at $z \sim 0.5$ in the GOODS fields. In the cases of Conselice et al. (2005), however, early-type galaxies were selected using a quantitative methods (concentration-asymmetry-clumpiness correlations), which possibly regard bulge-dominant late-type galaxies as early-type.

3.2. Selection of Blue Early-type Galaxies

We divided the sample of early-type galaxies into two groups: red early-type galaxies (REGs) and blue early-type galaxies (BEGs), using the $(i - z)_{\text{AB}}$ color variation as a function of redshift. REGs correspond to typical early-type galaxies seen in the local universe. The color of early-type galaxies varies significantly as redshift increases but the color evolution of typical REGs are approximately reproduced with the simple stellar population (SSP) model. Therefore, it is efficient to use the color difference between the observed color and the SSP expectation value for selecting BEGs.

Fig. 1 displays the $(i - z)$ color difference ($\Delta(i - z) \equiv (i - z)_{\text{model}} - (i - z)_{\text{obs}}$) vs. redshift for the sample of early-type galaxies. To derive $(i - z)_{\text{model}}$, we used the SSP model with formation redshift $z_{\text{F}} = 5$ (single-burst 12.4 Gyr ago) and metallicity $[\text{Fe}/\text{H}] = -0.4$ dex, calculated with the GALAXEV code (Bruzual & Charlot 2003). $[\text{Fe}/\text{H}] = -0.4$ dex was chosen because it matches well the observed colors of REGs. Several features are noted in Fig. 1. First, most galaxies at $z < 1.2$ are concentrated around the zero color difference, showing that their colors are well reproduced by the SSP model. Second, there are a significant number of galaxies with large positive color differences at $z < 1.2$, and all galaxies at $z > 1.2$ show even larger color differences. Third, one galaxy at $z \approx 0.75$ shows a large negative color difference, indicating that it may be a highly reddened galaxy.

In Fig. 1, we find no early-type galaxy that agrees with the SSP expectation at $z > 1.2$. This is because only rest-frame UV images can be seen at $z > 1.2$ in the GOODS bands and because typ-

ical early-type galaxies (i.e., REGs) are very faint in the UV wavelength.

Considering the features seen in Fig. 1, we divided the sample of galaxies at $z \leq 1.2$ as follows. First, we divided the redshift range of $0 \leq z \leq 1.2$ into five bins, and derived a color histogram of the galaxies for each redshift bin. In the left panel of Fig. 2, the redshift and $\Delta(i - z)$ values of the galaxies at $0 \leq z \leq 1.2$ are plotted. We divided this redshift range into five bins so that each bin contains a similar number of galaxies: $0 - 0.4$, $0.4 - 0.5$, $0.5 - 0.6$, $0.6 - 0.8$, and $0.8 - 1.2$. For each bin, we present an $(i - z)$ color difference histogram in the right panel of Fig. 2. The color difference histogram in each bin shows a strong peak around the $\Delta(i - z) = 0$, which can be fit well by a gaussian function. The galaxies around this peak correspond to the REGs. We derived a guideline for color separation by fitting a 3rd-order polynomial function to the colors corresponding to the peaks in the five bins. We regard as BEGs the early-type galaxies that are 3σ bluer than the peak color. Applying the criteria established above, we selected 113 REGs and 58 BEGs. This selection is not sensitive to the choice of evolutionary models, because the main criterion is the color distribution itself of early-type galaxies.

We checked the possibility that our BEG sample is biased to S/Irr types of Bundy et al. (2005) sample, and found that this is not that case: 64% of our BEGs are classified as E, E/S0, compact galaxy, or star by Bundy et al. (2005), which is just a little smaller than the ratio for our entire early-type sample.

Fig. 3 displays the $(i - z)$ color vs. redshift diagram of the REGs and the BEGs. We also plotted 1,778 galaxies classified as non-early-type for comparison. We plotted as well several evolutionary models with $[\text{Fe}/\text{H}] = -0.4$ and $z_{\text{F}} = 5$ given by Bruzual & Charlot (2003): an SSP model and three exponentially-decreasing star-formation rate models with exponential time-scales, $\tau = 0.5, 1$, and 8 Gyr.

Fig. 3 shows several important features of the REGs and the BEGs. 1) The REGs follow closely the SSP model up to $z \approx 1.2$. 2) The BEGs are found at $0 < z < 3.7$, while the REGs are found only at $z < 1.2$. 3) The color dispersion of the BEGs at given redshift is larger (ranging from $(i - z) \approx 0.2$ to 0.75 at $z \approx 1$) than that of the REGs,

as also seen in Fig. 2. 4) All BEGs at $z > 1.2$ are significantly bluer than the SSP model and their color evolution matches roughly the exponentially-decreasing star-formation rate models rather than the SSP model.

Table 1 lists the basic properties of the BEGs selected in this study: our short ID, IAU ID, spectroscopic redshift, and AB magnitudes in four bands. We used short IDs of ‘GN’ for GOODS-HDFN and ‘GS’ for GOODS-CDFS. The maximum photometric errors in our BEG sample are 0.055, 0.027, 0.027, and 0.015 for B, V, i , and z , respectively.

4. RESULTS

We have derived several physical parameters of the 58 BEGs and have investigated their morphological structures in comparison with those of the REGs.

4.1. Color-Magnitude Diagram

Fig. 4 displays the $(i - z)_{\text{AB}}$ vs. z_{AB} diagram of the BEGs in comparison with the REGs and non-early-type galaxies selected in this study. Fig. 4 shows following features. 1) The magnitudes of most BEGs range from $z_{\text{AB}} \approx 19.5$ to 23.7 , and two BEGs (GN 14242 and GS 895) are about 1.5 mag brighter than the rest of the BEGs. 2) The magnitudes of the REGs are in the similar range to those of the BEGs. 3) However, the BEGs are relatively bluer and fainter than the REGs so they can be roughly separated even in the observed color-magnitude diagram. 4) The colors of the REGs get redder as their redshift increases, while those of the BEGs at the low redshift and high redshift occupy a similar range.

4.2. Magnitudes and Sizes vs. Redshift

We have investigated the variation of the absolute magnitudes and sizes of the BEGs as a function of redshift in comparison with the REGs, which are listed in Table 2. Fig. 5 displays apparent z -band magnitude ($m_{z, \text{obs}}$), absolute z -band magnitude ($M_{z, \text{obs}}$), half-light radius ($R_{hl, z}$) in pixel and $R_{hl, z}$ in kpc. The typical estimation error of half-light radius, $\text{err}(R_{hl})$ is about $+4\%/-5\%$. We present the mean magnitudes and sizes of the BEGs and REGs as a function of the redshift in Fig. 5. Here we used the observer-frame

magnitudes instead of the rest-frame magnitudes, because the spectral energy distributions (SEDs) of the BEGs are too diverse to derive K-correction.

Several interesting features are noted in Fig. 5. 1) The absolute z -band magnitudes of the BEGs are fainter on average than those of the REGs. The differences in the maximum absolute z -band magnitudes between the BEGs and the REGs get smaller as the redshift increases, reaching almost zero at $z \approx 0.9$. The lower envelopes of the absolute magnitudes of the BEGs are affected by the magnitude limit, but the upper envelopes should be free of this. 2) The mean values of the half-light radii of the BEGs are smaller than those of the REGs. 3) While the half-light radii of REGs show little change as redshift increases until $z \approx 1.2$, those of the BEGs increase along redshift. 4) The half-light radii of the BEGs at $z > 1.2$ are smaller than 2 kpc. 5) Two brightest BEGs at $z \approx 0.5$ and ≈ 0.85 (GN 14242 and GS 895, respectively) are brighter than the brightest REGs at the same redshift, and their half-light radii are as large as the largest REGs.

Fig. 6 displays the absolute magnitude vs. the half-light radius of the REGs and the BEGs. It shows that both REGs and BEGs get brighter as they get larger. One remarkable feature in Fig. 6 is that the BEGs at $z > 1.2$ do not follow this correlation. They are very luminous in spite of their small sizes, showing a possibility that most BEGs found at $z > 1.2$ may contain AGNs.

We estimated roughly the masses of the sample galaxies, using galaxy evolution models of Bruzual & Charlot (2003) overlaid on the magnitude vs. redshift diagram, as shown in Fig. 7. Three kinds of galaxy evolution models were used: one SSP model with $z_F = 5$, one SSP model with $z_F = 2$, and one exponentially-decreasing star-formation rate model with $z_F = 5$ and $\tau = 8$ Gyr. In all models, the metallicity $[\text{Fe}/\text{H}] = -0.4$ was adopted. From the comparison of the data with the evolution models, we find the followings. 1) Using the SSP model with $z_F = 5$, we estimate the mass range of the REGs to be from $10^{10}M_\odot$ to $10^{12}M_\odot$. Most REGs have masses from $10^{11}M_\odot$ to $10^{12}M_\odot$. 2) It is not easy to estimate reliably the masses of the BEGs, because their star formation histories are not yet known. We used one SSP model with $z_F = 2$ and one exponentially-decreasing star-formation rate model with $z_F = 5$

and $\tau = 8$ Gyr for this. Using the SSP model with $z_F = 2$, we find the masses of most BEGs range from $10^{10}M_\odot$ to $10^{12}M_\odot$. More than half of them have masses lower than $10^{11}M_\odot$, and some even lower than $10^{10}M_\odot$. In summary, the BEGs have relatively lower masses than the REGs. However, it should be considered that faint spectra without strong lines (e.g. faint REGs) are harder to secure than faint spectra with strong lines (possibly faint BEGs), and that the superiority in magnitude, size and mass of REGs to BEGs shown in Fig. 5 and Fig. 7, can be partially caused by this spectroscopic bias.

Fig. 8 displays the number counts of the REGs and the BEGs, and the variation of the BEG fraction in the entire sample of early-type galaxies along redshift. The redshift distribution of the BEGs is almost flat at $z \leq 1.2$, whereas that of the REGs show a strong concentration at $z \approx 0.55$. (this concentration may be originated from the large-scale clustering seen in the GOODS fields; Conselice et al. 2005). No REG was found at $z > 1.2$ due to the limitation of optical observation, as mentioned in §3.2. The fraction of the BEGs to entire early-type galaxies is almost constant (~ 0.3) from $z = 0.1$ to $z = 1.1$, which is in good agreement with the result of Menanteau et al. (2004) based on the study of HST/ACS images of the UGC 10214 field. Noting that the target fields and the sample selection are different in these two studies, the agreement between the two results is remarkable. This indicates that the fraction of the BEGs in early-type galaxies may be constant at $z < 1.1$.

In Fig. 9, the half-light radius distribution (left panel) and the absolute magnitude distribution (right panel) of the REGs and the BEGs, respectively, are presented for four redshift bins. At first glance, these histograms show that the BEGs at lower redshift are smaller and fainter than the BEGs at higher redshift, unlike the REGs that keep almost consistent size and luminosity regardless of their redshift. However, we need to consider the following two points. First, since we did not conduct k-correction (neither photometrically nor morphologically), it can be affected by selection effect to compare sizes or magnitudes between different redshift bins directly. Therefore, we should focus on the *difference* between the BEGs and the REGs in each redshift bin, not the values them-

selves. Second, because magnitudes are dependent on the star-formation history as shown in Fig. 7, the magnitudes of REGs and BEGs may be different systematically if the BEGs have more recent-star-formations than the REGs. Moreover, exact k-corrections are necessary for fair comparison of magnitudes, which is hard to conduct for the BEGs. On the other hand, the size of a galaxy is affected by its dynamical history but relatively less affected by its star-formation history. When supposing typical velocity dispersions, size may represent the mass of a dynamically-stable system straightforwardly.

Considering those points, we compared the median sizes of the BEGs and the REGs in four redshift bins in Fig. 10. The upper-left panel of Fig. 10 displays how the median sizes of the REGs and the BEGs vary along redshift. In the z band, both the REGs and the BEGs enlarge as redshift increases. The size of the BEGs in the B band also shows an increasing trend along redshift, although there is a small reversion from $z \sim 0.5$ to $z \sim 0.7$. However, the size of the REGs in the B band becomes smaller as redshift increases. This is because the B band represents rest-frame UV wavelength at $z \sim 1$ and because typical REGs are very faint in the UV wavelength due to the lack of young stellar population.

In the lower-left panel of Fig. 10, the ratio of BEG median size to REG median size as a function of redshift is displayed. 1) In the z band, the BEG/REG median-size ratio evolves from 0.52 at $z \sim 1.0$ to 0.36 at $z \sim 0.2$. 2) In the B band images, the size ratio evolves more rapidly than in the z band, resulting that the size ratio at $z \sim 0.2$ is only 0.28 in spite of the extremely high ratio at $z \sim 1.0$. Considering the rest-frame wavelength of each redshift bin in each band, the B -band size ratio at $z \sim 0.2$ (0.28) that is even smaller than the z -band size ratio at $z \sim 1.0$ (0.52), confirms the size – redshift relation of the BEGs, free from the dependence of galaxy size on wavelength.

In addition to the wavelength effect, there is one more thing to be considered: the lower limit of observable size. If there are more faint BEGs undetected at $z \sim 1$ than faint REGs (although it is an opposite supposition to the possible spectroscopic bias mentioned above), this ‘small BEG missing’ can cause the overestimation of the BEG median size at $z \sim 1$. To avoid this effect, we

also used the 3rd largest galaxy sizes for both the REGs and the BEGs, which represent the upper envelope of galaxy size in each bin (the largest or the 2nd largest can be very sensitive to the existence of abnormally large objects). Since the 3rd largest galaxies are much brighter than the flux limit of any survey we referred up to $z \sim 1$ (by 3 – 4 mag; see Fig. 5), this parameter is almost free from observational biases. The result is presented in the upper-right and the lower-right panels of Fig. 10, which shows that the size ratio varies more rapidly than the median values. This result shows that the size evolution of the BEGs is not a selection effect caused by the lower envelope of observable magnitude. In summary, the BEGs at low redshift are *indeed* smaller (and maybe less massive) than the BEGs at intermediate redshift ($z \sim 1$). Recently, Ilbert et al. (2006) showed a similar trend, based on the evolution of galaxy luminosity function according to morphology up to $z = 1.2$ using VIMOS-VLT Deep Survey (Le Fèvre et al. 2004) and COMBO-17 (Meisenheimer & Wolf 2002) data: ‘blue bulge-galaxies’ are dimming by 0.7 mag from $z = 1$ to $z = 0.6$, which is in a good agreement with the size evolution of BEGs in our sample.

4.3. Structure

We display the gray-scale maps and isophotal contours of z -band images of the 58 BEGs in Fig. 11. Three typical REGs (GN10606, GN15469, and GN22886) with different apparent magnitudes ($m_z = 20.85, 18.87, \text{ and } 22.01$ respectively) are also displayed for comparison.

Fig. 11 shows that most BEGs look in general very similar to the REGs so it is difficult to distinguish them without colors. Only a few BEGs show slightly distorted or elongated isophotes in the central regions (GN14128, GN17606, GN19857, GN25594). We fitted the z -band images of the BEGs using the IRAF/ELLIPSE task. Fig. 12 displays the surface brightness profiles of the BEGs and three REGs for comparison. Since the profiles within the PSF radius are flat, we fitted the surface brightness profiles of outer regions of the galaxies with the de Vaucouleur ($R^{1/4}$) law. In Fig. 12, the surface brightness profiles of outer regions of most BEGs are fit well by the de Vaucouleur law like those of the REGs. Thus there is little difference in the images and surface bright-

ness profiles between the BEGs and the REGs.

4.4. Color Maps

We created pseudo-color maps representing the $(V - i)$ color of the BEGs using V and i images, as shown in Fig. 13. Strikingly diverse features of the BEGs are noted in Fig. 13.

A blue clump (BC) mostly in the central regions of the galaxies is one conspicuous feature of many BEGs. There are several types of blue clumps found in Fig. 13: a symmetric deep BC (i.e., a steep blue dip in the color profile; e.g., GN1430, GN5302, and GS20457); a symmetric shallow BC (i.e., shelving inverse color gradient in the color profile; e.g. GN14229, GS13482, and GS21636); an asymmetric (or elongated) BC (e.g., GN8292, GN21983, and GS9479); an off-centered BC (e.g. GN10598, GN16895, and GS7517); and multiple BCs (GN28407). For a typical massive REG, it is well known that its color profile shows a negative color gradient (i.e., its central part is redder than its outer part) probably originated from its internal metallicity gradient (Tamura et al. 2000), and a blue clump is hardly found in bright REGs. A blue clump may represent the existence of a large amount of young stellar population or, for some deep BCs, may represent the existence of an AGN in the center of the BEG.

In addition to blue clumps, other kinds of remarkable features are found in the outer regions of BEGs. Although the intensity maps of BEGs show good elliptical or circular shapes in Fig. 11, the pseudo-color maps in Fig. 13 reveal diverse faint structures in the BEGs: 1) tidally distorted outer structures (e.g., GN1430, GN9126, and GN10598); 2) very nearby (and maybe interacting) objects (e.g., GN5302, GN7904, and GS17085); 3) a red inner ring (e.g., GN19996, GS10754, and GS20457); and 4) a blue outer ring (GN11421). The tidally distorted outer structures and the very nearby companions indicate that those BEGs may be under the tidal influence from other objects, probably responsible for the blue stellar population.

The nature and origin of the red inner ring are difficult to explain. One possibility is that they are artificial features resulted from the PSF variation according to ACS bands (see Appendix B in Menanteau et al. (2004)). However, the red inner

ring features are conspicuous both in the $(V - i)$ color maps and in the $(V - z)$ color maps, and their positions and sizes are almost identical in the two kinds of color maps. If they are indeed the results of PSF variation, the shapes of the rings in each color map may be significantly different from each other. Therefore, the red inner rings are considered to be real features.

GN11421, the BEG with a blue outer ring, shows an interesting morphological variation along wavelength. The properties of the ring galaxies at high redshift including not only GN11421 but also two other GOODS objects will be described in the Appendix. A possible origin of the ring feature of GN11421 is a head-on collision between two galaxies (Appleton et al. 1996).

We used the $(V - i)$ color maps to investigate the fine color structures of BEGs, to minimize the effects caused by different PSF FWHMs in different bands. It is generally known that the ACS z -band FWHM is wider than those of B , V , and i bands (Menanteau et al. 2004). (The reason we did not use the B band images is that many BEGs are too faint in the B band.) However, since $(V - z)$ color can show fine color structures more conspicuously than $(V - i)$ color owing to its wide wavelength interval, we checked the difference between the features in the $(V - i)$ color maps and those in the $(V - z)$ color maps. Most major features are not much different in the two color maps, but the shapes of some central BCs look slightly different in different colors. Some asymmetric features of central BCs are too conspicuous to be artifacts, but some may result from the effect of PSF variation according to bands. In the $(V - z)$ color map, it is interesting that GN14128 with an off-centered core in the contour map has a blue clump biased toward the opposite direction to the bright core seen in the z band, which is good evidence for the tidal event of GN14128 and is not seen in the $(V - i)$ color map.

Fig. 14 displays the $(V - z)$ color profiles of the 58 BEGs and three REGs. We inspect the $(V - z)$ color profiles not the $(V - i)$ color profiles, because it is more advantageous to use colors with a wider wavelength interval in investigating radial variations of stellar population, and because the PSF variation effect may be not significant except within the small central regions in the surface profiles of galaxies. In Fig. 14, the

brightest one (GN15469; $M_z = -22.13$) among the three REGs shows almost flat color profile and the intermediately-bright REG (GN10606; $M_z = -21.33$) also has an almost flat color profile with small scatters, while the faintest one (GN22886; $M_z = -18.75$) shows a very weakly-blue center. Compared with these REGs, the BEGs have very diverse color profiles: some BEGs (e.g., GN14242, GN16895, and GS895) are not much different from the bright REGs; some BEGs (e.g., GN9126, GN14128, and GS13482) have just shallow BCs like the faint REG; and some BEGs (e.g., GN5302, GN19996, and GS20048) have very deep BCs that are not found in the REGs. In addition, the color profiles of some BEGs do not vary monotonically: the color profiles in some BEGs vary from increasing to constant (e.g. GN13334 and GS20048); the color profiles in some other BEGs vary from constant to increasing (e.g., GN17217 and GS28929); and the color profiles in other BEGs undulate (e.g., GS6587 and GS11796). The complex color profile may indicate the complex spatial distribution of the stellar populations in the BEG. The features found in the pseudo-color maps are summarized in Table 3.

4.5. X-ray Luminosity and Spectral Line Feature

We calculated the X-ray luminosity of the BEGs that have X-ray flux data, adopting a typical AGN SED, as listed in Table 3. It is generally known that an AGN generates strong X-ray emission (Elvis et al. 1978) and that vigorous star-formation activities can also lead to X-ray emission (Laird et al. 2005). The criterion is somewhat ambiguous, for distinguishing between X-ray emission from an AGN and X-ray emission from star formation activity. We divided the sample of BEGs into low X-ray luminosity objects ($L_{0.5-10\text{keV}} < 10^{43.5}$ erg s $^{-1}$) and high X-ray luminosity objects ($L_{0.5-10\text{keV}} \geq 10^{43.5}$ erg s $^{-1}$). This separation is based on the fact that the maximum X-ray luminosity of the ‘spectroscopic non-AGNs’ (see below) in our sample is $10^{43.34}$ erg s $^{-1}$. Fig. 15 shows these X-ray luminosity features on the $\Delta(i-z)$ vs. redshift diagram. The X-ray BEGs are found only at $z > 0.5$ and their $\Delta(i-z)$ values range from very small (≈ 0.15) to very large (≈ 1.15). It is remarkable that nine of the thirteen BEGs at $z > 1.2$ have high X-ray

luminosity, implying that most BEGs at $z > 1.2$ may be probable AGN-host galaxies.

Using the spectra, we classified the CDFS BEGs according to their spectral line features into four categories: absorption line galaxies, emission line galaxies, composite line galaxies, and AGNs, as listed in Table 3. Fig. 16 displays the spectral line features on the $\Delta(i-z)$ vs. redshift diagram. The following features are noted. 1) There are six absorption-line BEGs: four with $(i-z) < 0.35$ at $z < 0.8$ and two with $0.5 < (i-z) < 0.6$ at $z \approx 1$ and 1.5. 2) Non-AGN objects are found only at $\Delta(i-z) < 0.6$. 3) Some emission-line BEGs and composite-line BEGs have smaller $\Delta(i-z)$ than the average $\Delta(i-z)$ of absorption-line BEGs. Since emission lines in a galaxy are generally a good indicator of the star-formation activity or AGN activity, this indicates that most BEGs probably contain ongoing star-formation or an AGN.

We checked the correlation between the blue clumps and the X-ray luminosity, finding a significant coincidence between ‘a symmetric deep blue clump or an elongated blue clump’ and ‘X-ray emission’. There are eleven BEGs with $L_{0.5-10\text{keV}} \geq 10^{43.5}$ erg s $^{-1}$ (hereafter, *X-ray luminous*) and 16 BEGs with a deep blue clump (hereafter, *blue clumpy*). Among them, ten BEGs are both *X-ray luminous* and *blue clumpy*; in other words, 91% of *X-ray luminous* BEGs are *blue clumpy* and 63% of *blue clumpy* BEGs are *X-ray luminous*.

We also checked the correlation between the X-ray luminosity and the spectral line features, finding four of eight ‘spectroscopic AGNs’ (GS467, GS3739, GS20244, and GS22653) are *X-ray luminous* BEGs. One spectroscopic AGN GS20457 did not match any X-ray source, and the other three spectroscopic AGNs (GS6961, GS13482, and GS20048) are in the X-ray luminosity range of $10^{42.35} \leq L_{0.5-10\text{keV}} \leq 10^{43.14}$, implying possible existence of more AGNs with low X-ray luminosity.

5. DISCUSSION

5.1. The Nature of the BEGs

In the previous studies, blue E/S0 galaxies were regarded as: 1) star-forming low-mass spheroids with inverse color gradients (Im et al. 2001); 2) early-type galaxies with a blue central clump

caused by prolonged single-collapse (Menanteau et al. 2001b) or caused by the accretion of blue objects (Elmegreen et al. 2005a); 3) early-type galaxies that suffered the secondary starburst (Ferreras et al. 2005); or 4) AGN-host galaxies (Menanteau et al. 2005). In this study, we found the followings, focusing on the fine structures of the blue early-type galaxies.

First, at least 47% (27/58) of the BEGs have traces of tidal interactions (an elongated or off-centered core; an elongated or off-centered blue clump; multiple blue clumps; tidally distorted outer structures; interacting companions; or a blue outer ring).

Second, at least 28% (16/58) of the BEGs probably contain AGNs in their centers (high X-ray luminosity or AGN spectra). This result supports the idea that AGNs may be responsible for the blue color of some blue E/S0 galaxies (Menanteau et al. 2005). It is interesting that 14% (8/58) of the BEGs (GN1430, GN5302, GN8292, GN24520, GN24667, GS3739, GS20048, and GS22653) show both the traces of tidal events and the AGN features, because this partially supports the merger origin of AGNs (Canalizo 2001; Kewley & Dopita 2003; Sánchez et al. 2005).

Third, 19% (11/58) of the BEGs have red inner rings whose nature is still unclear. All of these red-ring BEGs are *blue clumpy* and 69% (11/16) of the *blue clumpy* BEGs have red inner rings. This indicates that the red inner rings are possibly related to AGN activity or strong star-formation activity. However, it is not easy to explain how such rings form in detail.

Fourth, as described in §4.2, the BEGs have smaller sizes than the REGs on the average. However, there are also several BEGs with large sizes: 22% (13/58) of the BEGs are larger than $R_{\text{hl},z} = 2$ kpc and two BEGs (GN14242 and GS895) are even as large as $R_{\text{hl},z} \approx 10$ kpc. Considering such large sizes of those BEGs, they are hardly ‘star-forming low-mass spheroids (Im et al. 2001)’ unless they are very unstable dynamically or their velocity dispersions are unusually small.

Almost a half of the BEGs show evidence of tidal events and at least a quarter of the BEGs probably contain an AGN in their center. At least in our sample, the role of extra-galactic disturbance appears to be more dominant than that

of a prolonged single collapse (Menanteau et al. 2001b). Within the frame of the ‘two-burst model’ (Ferreras et al. 2005), the ‘secondary burst’ may be interpreted as the result of a tidal interaction or merging with other objects.

5.2. BEGs and Galactic *Downsizing* model

Recently, evidences are accumulating, supporting a new scheme for early-type galaxy formation: the galactic *downsizing* (Cowie et al. 1996; Susa & Umemura 2000; Treu et al. 2005). According to the *downsizing* model, the more massive galaxies are, the older they are. Although this scenario started as a modified version of the monolithic collapse model, it was suggested more recently that the *downsizing* can be also compatible with the hierarchical merging scenario. Bundy et al. (2005) found that the E/S0 fraction decreases as redshift increases, while the stellar mass function for all galaxies shows little evolution. At the same time, they also found that the lower-mass limit of E/S0 galaxies is higher at earlier epoch, which indicates that galaxy merging may be significantly related to the *downsizing* scheme. Faber et al. (2006) supported this idea with the evolution of the luminosity function for blue and red galaxies to $z \sim 1$ using the DEEP2 (Davis et al. 2003) and the COMBO-17 (Wolf et al. 2003) survey data. According to them, the ‘quenching mass’ from blue galaxies to red galaxies via gas-rich mergers, decreases as time goes. De Lucia et al. (2006) showed that it is possible to reproduce the *downsizing* using the simulation based on the hierarchical merging scenario and the Λ CDM model.

Interestingly, the BEGs in our sample also show some relationship with the *downsizing* model in their size – redshift relation, as shown in Fig. 9 and Fig. 10: the BEGs at lower redshift are smaller than the BEGs at higher redshift, while the size of the REGs does not vary significantly with redshift. Because the BEGs have very similar morphological properties to the REGs (elliptical shape and $R^{1/4}$ surface brightness profile) and because there is no conspicuous discontinuity between the REGs and the BEGs (as shown in Fig. 2 and Fig. 3), it may be concluded that the BEGs will evolve into REGs. Evidence of recent star-formation in nearby early-type galaxies also supports this idea (Ferrarese et al. 2006; Kaviraj et al. 2006). On that assumption, the size – redshift relation

of BEGs seems to indicate that the mass of the BEG-REG migration decreases as time goes, supporting the ‘quenching mass decreasing with time’ suggested by Faber et al. (2006). According to this scenario, BEGs may be the intermediate objects from blue galaxies (late-type galaxies) to red galaxies (early-type galaxies).

For small blue E/S0 galaxies, however, a new explanation was suggested. Ferreras et al. (2005) regarded the faint blue E/S0 galaxies as a different population from the bright blue E/S0 galaxies, on the basis of the low surface brightness of the faint blue E/S0 galaxies. Ferreras et al. (2005) concluded that the faint blue E/S0 galaxies may be spirals with strong starbursts, whereas the bright blue E/S0 galaxies will probably evolve into normal red E/S0 galaxies. However, if the small BEGs are really late-type galaxies with very faint disks and spiral arms, the visible parts of them are probably galactic bulges, whose color is typically red due to old stellar populations (Zoccali et al. 2003) unlike the color of the small BEGs. Another possible explanation is that they may be the ‘progenitors’ of late-type galaxies. According to the ‘spiral rebuilding’ scenario suggested by Hammer et al. (2005), normal spiral galaxies may evolve and grow through the phases of ‘merger’ – ‘compact galaxy’ – ‘disk growth’, from $z \approx 1$ to $z \approx 0.4$. The small BEGs are possibly matched with objects in the ‘compact galaxy’ phase. However, this explanation also has two weak points. First, many small BEGs are found at even $z < 0.4$ in our sample. In addition, the ‘spiral rebuilding’ scenario does not explain the size of the spiral bulges decreasing with time, which is the opposite of the prediction of that scenario.

A good possibility for the destiny of the small BEGs is that they may evolve into dwarf elliptical galaxies. Ilbert et al. (2006) also predicted that ‘blue bulge-galaxies’ may evolve into local dwarf spheroidal galaxies. Interestingly, this inference is consistent with the *downsizing* scheme in the formation of early-type galaxies. By analyzing the luminosity vs. surface brightness relation of bright and dwarf elliptical galaxies, Graham & Guzman (2003) showed that there is no intrinsic gap between bright elliptical galaxies and dwarf elliptical galaxies, and that they may be one continuous population just with different masses, unlike the traditional belief that there is a dichotomy

between the two galaxy populations (Kormendy 1977, 1985). In addition, Ferrarese et al. (2006) showed that there is no clear bimodality between dwarf and regular elliptical galaxies in the surface brightness profile and isophotal parameters, in their analysis of 100 early-type galaxies in the Virgo cluster using HST/ACS. In this viewpoint, BEGs are probably the progenitors of normal and dwarf elliptical galaxies, mostly originated from mergers/interacting-galaxies or AGNs.

6. CONCLUSION

In this paper, we present a study of the properties of BEGs in the GOODS HST/ACS fields. We selected 171 early-type galaxies visually in the GOODS HST/ACS archival data with spectroscopic redshift. We divided the early-type galaxies into 58 BEGs and 112 REGs using their $(i - z)_{AB}$ color distribution at given redshift. The BEGs have well-defined elliptical shapes and $R^{1/4}$ surface profiles similar to the REGs, with just a few exceptions. However, the analysis of internal color distribution, X-ray luminosity, and spectral line features show that almost a half of the BEGs have evidence of tidal events and at least a quarter of the BEGs probably contain an AGN in their centers. From the analysis of the size and magnitude of the BEGs and the REGs, we have found the evidence that the sizes of BEGs are decreasing as redshift decreases, which is consistent with the *downsizing* scenario with hierarchical merging.

We conclude that the BEGs may be primarily descendants of past merger/interacting-galaxies and secondarily the AGN-host early-type galaxies, and that BEGs may evolve into normal or dwarf elliptical galaxies. However, there are still several open questions to answer. First, we could not find any BEGs at $z > 1.2$ as large as REGs. If larger REGs formed at the higher redshift and if all REGs were BEGs at one time, many BEGs as large as giant REGs are expected to exist at $z > 1.2$. Therefore, the question is whether all REGs evolved from BEGs or not. If not, what is the difference between those two (or more) building processes of early-type galaxies? The mechanism that makes the central deep blue clumps in almost a half of the BEGs is another question. It is hard to tell whether all *blue clumpy* BEGs contain AGNs or not, since the X-ray detection or

matching with optical catalog is limited. Deep observation in other bands (e.g., mid-infrared spectroscopy using JWST (Rieke et al. 2005), which may enable to identify the PAH emission of faint objects) will be helpful to resolve which is dominant in the blue clumps between AGN activity and star-forming activity. In addition, the origin of the red inner rings in some BEGs is also a mystery to be solved with further studies.

The authors are grateful to Myungshin Im, Won-Kee Park, Narae Hwang, and Minjin Kim for constructive suggestions, and to anonymous referee for very useful comments. This paper is in part supported by the grant (R01-2004-000-10490-0) from the Basic Research Program of the Korea Science & Engineering Foundation. This paper is based on observations with the NASA/ESA *Hubble space telescope*, obtained at the Space Telescope Science Institute, which is operated by the Association of Universities for Research in Astronomy, Inc. under NASA contract NAS 5-26555. The HST/ACS observations are associated with proposals 9425 and 9583.

A. RING GALAXIES IN THE GOODS FIELDS

We have found three ring galaxies in the GOODS fields, including one BEG with an outer UV ring, GN11421 (GDS J123640.02+621207.7). The other two ring galaxies, GN5542 (GDS J123618.94+620844.4) and GN26250 (GDS J123729.85+621645.2) have very similar morphological properties with GN11421. However, their rings can be identified not only in the rest-frame UV band images but also in the rest-frame optical band images. Therefore, GN5542 and GN26250 were not included in our sample of early-type galaxies.

Fig. 17 shows the morphological variations along wavelength of the three ring galaxies. The three ring galaxies look almost spheroidal or elliptical in the z band. The shorter the wavelength is, however, the smaller their central spheroids are and the brighter their outer rings appear. GN5542 and GN26250 show more dramatic variations than GN11421: the central spheroids of GN5542 and GN26250 almost disappear in their B band images. Assuming that the rings are circular and that they look elliptical due to inclination, the diameters of the rings are estimated to be 5 kpc for GN5542 and GN11421, and 8 kpc for GN26250. These values are relatively small compared to the sizes of nearby ring galaxies (5–52 kpc; Theys & Spiegel 1976).

Ring galaxies in the nearby universe (e.g., the famous Cartwheel galaxy) have been known for long. Appleton et al. (1996) explained that a ring galaxy may be the result of a head-on collision between ‘a target galaxy’ and ‘an intruder’. According to their observational and numerical studies, a ring wave that rotates and expands, occurs in the target galaxy after the massive and compact intruder penetrates the target galaxy. The V band image of GN26250 is surprisingly similar to that of the *Cartwheel* galaxy that is a representative collisional ring galaxy. Therefore these distant ring galaxies were also probably formed by the same process. To our knowledge, GN11421 ($z = 1.015$) is the most (or at least one of the most) distant ring galaxy ever found to date. The most distant ring galaxy in the previous sample of Lavery et al. (2004) is at $z = 0.996$.

REFERENCES

- Abraham, R. G., Ellis, R. S., Fabian, A. C., Tanvir, N. R., & Glazebrook, K. 1999, *MNRAS*, 303, 641
- Alexander, D. M., et al. 2003, *AJ*, 126, 539
- Appleton, P. N., Charmandaris, V., & Struck, C. 1996, *ApJ*, 468, 532
- Beckwith, S. V. W., et al. 2003, *Bulletin of American Astronomical Society Meeting*, 202, 17.05
- Bertola, F., & Capaccioli, M. 1975, *ApJ*, 200, 439
- Bruzual, G., & Charlot, S. 2003, *MNRAS*, 344, 1000
- Bundy, K., Ellis, R. S., & Conselice, C. J. 2005, *ApJ*, 625, 621
- Bunker, A. J., Stanway, E. R., Ellis, R. S., McMahon, R. G., & McCarthy, P. J. 2003, 342, L47
- Canalizo, G. 2001, *BAAS*, 33, 831
- Cohen, J. G., Hogg, D. W., Blandford, R., Cowie, L. L., Hu, E., Songaila, A., Shopbell, P., & Richberg, K. 2000, *ApJ*, 538, 29
- Conselice, C. J., Blackburne, J. A., & Papovich, C. 2005, *ApJ*, 620, 564
- Cowie, L. L., Barger, A. J., Hu, E. M., Capak, P., & Songaila, A. 2004, *AJ*, 127, 3137
- Cowie, L. L., Songaila, A., Hu, E. M., & Cohen, J. G. 1996, *AJ*, 112, 839
- Cristiani, S., et al. 2000, *A&A*, 359, 489
- Croom, S. M., Warren, S. J., & Glazebrook, K. 2001, *MNRAS*, 328, 150
- Davis, R. L., Efstathiou, G., Fall, S. M., Illingworth, G., & Schechter, P. L. 1983, *ApJ*, 26, 41
- Davis, M., et al. 2003, *Proc. SPIE* 4834, 161
- Dawson, S., Stern, D., Bunker, A. J., Spinrad, H., & Dey, A. 2001, *AJ*, 122, 598
- De Lucia, G., Springel, V., White, S. D. M., Croton, D., & Kauffmann, G. 2006, *MNRAS*, 366, 499
- De Vaucouleurs, G. 1948, *Ann. Astrophys.*, 11, 247
- Dickinson, M., et al. 2003, in *Proc. of the ESO/USM Workshop "The Mass of Galaxies at Low and High Redshift"* (Venice, Italy, October 2001), ed. R. Bender, & A. Renzini (*astro-ph/0204213*)
- Dickinson, M., et al. 2004, *ApJ*, 600, L99
- Elmegreen, D. M., Elmegreen, B. G., & Ferguson, T. E. 2005a, *ApJ*, 623, L71
- Elmegreen, D. M., Elmegreen, B. G., Rubin, D. S., & Schaffer, M. A. 2005b, *ApJ*, 631, 85
- Elvis, M., Maccacaro, T., Wilson, A. S., Ward, M. J., Penston, M. V., Fosbury, R. A. E., & Perola, G. C. 1978, *MNRAS*, 183, 129
- Faber, S. M., & Gallagher, J. S. 1976, *ApJ*, 204, 365
- Faber, S. M., & Jackson, R. E. 1976, *ApJ*, 204, 668
- Faber, S., et al. 2006, *ApJ*, submitted (*astro-ph/0506044*)
- Ferrarese, L., et al. 2006, *ApJS*, in press (*astro-ph/0602297*)
- Ferreras, I., Lisker, T., Carollo, M., & Lilly, S. J. 2005, *ApJ*, 635, 243
- Franx, M., Illingworth, G., & Heckman, T. 1989, *AJ*, 98, 538
- Giacconi, R., et al. 2002, *ApJS*, 139, 369
- Giavalisco, M., et al. 2004, *ApJ*, 600, L93
- Graham, A. W., & Guzman, R. 2003, *AJ*, 125, 2936
- Groth, E. J., et al. 1994, *BAAS*, 185, 5309
- Hammer, F., Flores, H., Elbaz, D., Zheng, X. Z., Liang, Y. C., & Cesarsky, C. 2005, *A&A*, 430, 115
- Ilbert, O., et al. 2006, *A&A*, in press (*astro-ph/0604010*)
- Illingworth, G. 1977, *ApJ*, 218, L43

- Im, M., Faber, S. M., Gebhardt, K., Koo, D. C., Phillips, A. C., Schiavon, R. P., Simard, L., & Willmer, C. N. A. 2001, *AJ*, 122, 750
- Jørgensen, I., Franx, M., & Kjærgaard, P. 1993, *ApJ*, 411, 34
- Kaviraj, S., et al. (2006) *ApJ*, submitted (astro-ph/0601029)
- Kewley, L. J. & Dopita, M. A. 2003, *RevMexAA*, 17, 83
- Kormendy, J. 1977, *ApJ*, 218, 333
- Kormendy, J. 1985, *ApJ*, 295, 73
- Laird, E. S., Nandra, K., Adelberger, K. L., Steidel, C. C., & Reddy, N. A. 2005, *MNRAS*, 359, 47
- Larson, R. B. 1974, *MNRAS*, 166, 585
- Lavery, R. J., Remijan, A., Charmandaris, V., Hayes, R. D., & Ring, A. A. 2004, *ApJ*, 612, 679
- Le Fèvre, O., Vettolani, G., Paltani, S., Tresse, L., Zamorani, G., Le Brun, V., & Moreau, C. 2004, *A&A*, 428, 1043
- Lee, M. G. 2003, *JKAS*, 36, 189
- Lucey, J. R., Bower, R. G., & Ellis, R. S. 1991, *MNRAS*, 249, 755
- Meisenheimer, K., & Wolf, C. 2002, *Astronomy & Geophysics*, 43, 15
- Menanteau, F., Abraham, R. G., & Ellis, R. S. 2001a, *MNRAS*, 322, 1
- Menanteau, F., Ellis, R., Abraham, R., Berger, A., & Cowie, L. 1999, *MNRAS*, 309, 208
- Menanteau, F., Jimenez, R., & Matteucci, F. 2001b, *ApJ*, 562, L23
- Menanteau, F., et al. 2004, *ApJ*, 612, 202
- Menanteau, F., et al. 2005, *ApJ*, 620, 697
- Partridge, R. B., & Peebles, P. J. E. 1967, *ApJ*, 147, 868
- Rieke, G. H., Wright, G. S., and MIRI Science Team 2005, *Bulletin of American Astronomical Society Meeting*, 207, 115.18
- Sánchez, S. F., Becker, T., Garcia-Lorenzo, B., Benn, C. R., Christensen, L., Kelz, A., Jahnke, K., & Roth, M. M. 2005, *A&A*, 429, L21
- Searle, L., & Zinn, R. 1978, *ApJ*, 225, 357
- Stanway, E. R., Bunker, A. J., McMahon, R. G., Ellis, R. S., Treu, T., & McCarthy, P. J. 2004a, *ApJ*, 607, 704
- Stanway, E. R., et al. 2004b, *ApJ*, 604, L13
- Steidel, C. C., Adelberger, K. L., Shapley, A. E., Pettini, M., Dickinson, M., & Giavalisco, M. 2003 *ApJ*, 592, 728
- Strogler, L.-G., et al. 2004, *ApJ*, 613, 200
- Susa, H. & Umemura, M. 2000, *ApJ*, 537, 578
- Szokoly, G. P., et al. 2004, *ApJS*, 155, 271
- Tamura, N., Kobayashi, C., Arimoto, N., Kodama, T., & Ohta, K. 2000, *AJ*, 119, 2134
- Theys, J. C. & Spiegel, E. A. 1976, *ApJ*, 208, 650
- Tinsley, B. M. 1972, *ApJ*, 178, 319
- Toomre, A. 1977, in *The Evolution of Galaxies and Galaxy Populations*, ed. B. M. Tinsley & R. B. Larsen (New Haven: Yale University), 401
- Treu, T., Ellis, R. S., Liao, T. X., & van Dokkum, P. G. 2005, *ApJ*, 622, L5
- van der Wel, A., Franx, M., van Dokkum, P. G., & Rix, H.-W. 2004, *ApJ*, 601, L5
- Vanzella, E., et al. 2005, *A&A*, 434, 53
- Vigroux, L., Souviron, J., Lachieze-Rey, M., Vader, J. P., 1988, *A&AS*, 73, 1
- Visvanathan, N., & Sandage, A. 1977, *ApJ*, 216, 214
- Williams, R. E., et al. 1996, *AJ*, 112, 1335
- Wolf, C., Meisenheimer, K., Rix, H. -W., Borch, A., Dye, S., & Kleinheinrich, M. 2003, *A&A*, 401, 73
- Zoccali, M., et al. 2003, *A&A*, 399, 931

This 2-column preprint was prepared with the AAS L^AT_EX macros v5.2.

TABLE 1
BASIC PROPERTIES OF BEGs

ID (1)	IAU ID (2)	z_{spec} (3)	B_{435} (4)	V_{606} (5)	i_{775} (6)	z_{850} (7)
GN 1430	GDS J123557.62+621024.7	3.068	23.812	22.714	22.572	22.622
GN 3390	GDS J123603.62+621513.2	0.784	24.585	23.296	21.941	21.490
GN 5302	GDS J123617.99+621635.3	0.679	21.973	21.152	20.460	20.183
GN 7756	GDS J123627.32+621258.1	1.218	23.776	23.321	22.773	22.211
GN 7904	GDS J123627.86+621124.8	0.517	22.983	22.304	21.469	21.160
GN 8292	GDS J123629.44+621513.3	3.652	25.920	24.623	23.886	23.701
GN 9126	GDS J123632.56+620800.2	1.994	24.110	24.249	23.747	23.563
GN 10598	GDS J123637.32+620831.2	0.972	23.821	23.403	22.380	21.704
GN 11103	GDS J123638.98+620912.1	0.342	23.740	23.170	22.870	22.781
GN 11216	GDS J123639.30+621552.6	0.521	25.109	24.021	23.290	23.089
GN 11421	GDS J123640.02+621207.7	1.015	24.729	23.614	22.429	21.694
GN 12216	GDS J123642.49+621543.2	2.450	25.677	23.844	22.774	22.458
GN 13334	GDS J123646.34+621405.0	0.961	23.873	22.657	21.571	20.865
GN 14128	GDS J123649.06+621512.7	0.457	24.418	23.468	22.886	22.665
GN 14229	GDS J123649.37+621311.6	0.476	23.594	22.774	22.207	22.007
GN 14242	GDS J123649.43+621347.2	0.852	20.140	18.831	18.262	17.992
GN 15003	GDS J123651.65+620954.9	0.136	22.434	21.777	21.406	21.334
GN 15671	GDS J123653.52+622018.9	1.023	26.015	25.121	23.853	23.159
GN 16895	GDS J123657.34+621026.4	0.846	25.135	24.143	22.955	22.479
GN 17217	GDS J123658.30+621214.5	1.020	24.053	23.845	23.327	23.069
GN 17606	GDS J123659.48+620815.0	0.116	22.034	21.365	21.027	20.927
GN 19857	GDS J123706.96+621208.4	0.693	24.878	24.615	24.004	23.731
GN 19996	GDS J123707.49+622148.1	1.451	22.971	22.803	22.382	22.026
GN 21633	GDS J123713.22+621405.0	0.441	24.644	23.427	22.795	22.602
GN 21983	GDS J123714.39+621221.5	1.084	25.353	24.500	23.608	22.895
GN 24520	GDS J123723.19+621538.7	2.240	24.784	24.477	24.044	23.736
GN 24667	GDS J123723.72+622113.3	3.524	25.174	23.957	23.634	23.621
GN 25431	GDS J123726.64+621104.4	0.212	22.680	21.713	21.289	21.140
GN 25594	GDS J123727.34+621319.2	0.513	22.973	22.513	21.958	22.107
GN 28407	GDS J123739.49+621847.8	0.337	23.591	22.762	22.554	22.352
GN 31118	GDS J123757.31+621627.8	2.922	23.685	22.471	21.982	21.872
GS 467	GDS J033200.35-274319.7	1.037	22.705	22.348	22.214	22.033
GS 895	GDS J033202.71-274310.8	0.493	20.425	19.000	18.438	18.164
GS 1036	GDS J033203.29-274511.4	0.543	25.146	24.433	23.781	23.616
GS 1222	GDS J033204.10-274424.0	0.117	24.173	23.763	23.604	23.649
GS 3739	GDS J033210.91-274414.9	1.615	23.685	22.951	22.371	22.371
GS 5632	GDS J033214.68-274337.1	0.976	25.121	24.364	23.478	23.017
GS 6321	GDS J033215.98-274422.9	0.735	24.570	23.140	21.889	21.502
GS 6587	GDS J033216.49-275019.9	0.407	24.859	23.553	22.899	22.729
GS 6961	GDS J033217.14-274303.3	0.569	23.103	21.744	20.840	20.566

TABLE 1—*Continued*

ID (1)	IAU ID (2)	z_{spec} (3)	B_{435} (4)	V_{606} (5)	i_{775} (6)	z_{850} (7)
GS 7517	GDS J033218.05–275000.8	1.474	24.924	24.356	23.693	23.465
GS 8047	GDS J033219.00–274755.5	0.670	26.385	24.929	23.759	23.459
GS 9479	GDS J033221.51–275359.7	0.966	25.810	24.502	23.775	23.348
GS 10754	GDS J033223.66–275600.7	0.495	24.439	23.295	22.871	22.752
GS 11796	GDS J033225.29–274224.2	0.613	24.595	23.145	22.435	22.239
GS 12120	GDS J033225.77–274501.8	0.266	23.045	22.487	22.205	22.198
GS 13482	GDS J033227.62–274144.9	0.665	24.050	22.803	21.613	21.302
GS 17085	GDS J033232.96–274545.7	0.957	22.714	21.051	20.164	19.838
GS 20048	GDS J033237.46–274000.1	0.666	23.524	22.902	22.155	21.856
GS 20244	GDS J033237.76–275212.3	1.603	25.215	24.831	24.111	23.540
GS 20457	GDS J033238.12–273944.8	0.837	20.934	20.526	20.630	20.432
GS 21636	GDS J033240.04–274418.6	0.522	23.360	21.780	20.900	20.623
GS 22653	GDS J033241.85–275202.5	3.610	24.350	22.885	22.403	22.430
GS 23362	GDS J033243.24–274914.2	0.743	22.405	22.893	22.543	22.485
GS 24938	GDS J033246.73–275352.9	0.214	24.975	24.088	23.665	23.563
GS 27149	GDS J033252.39–275105.6	0.574	23.751	23.332	22.796	22.815
GS 27611	GDS J033253.65–275319.0	0.734	25.033	24.571	23.894	23.697
GS 28929	GDS J033258.71–275206.2	0.406	24.902	23.766	23.212	23.031

NOTE.—(1) Object MOSAIC ID number in the GOODS HST/ACS official catalog ver1.1 (‘GN’ for GOODS-HDFN and ‘GS’ for GOODS-CDFS); (2) Official name of IAU; (3) Spectroscopic redshift; (4) – (7) AB AUTO magnitudes provided in the GOODS HST/ACS official catalog ver1.1. The maximum photometric errors are 0.055, 0.027, 0.027, and 0.015 for B , V , i , and z , respectively.

TABLE 2
ADDITIONAL PROPERTIES OF BEGs

ID	$m - M$	M_z	$R_{hl,z}$ (pixel)	$R_{hl,z}$ (kpc)	$\Delta(i - z)_{SSP}$	$\Delta(i - z)_{crit}$
(1)	(2)	(3)	(4)	(5)	(6)	(7)
GN 1430	47.09	-24.47	4.5	1.034	0.65	—
GN 3390	43.45	-21.96	8.0	1.793	0.16	0.05
GN 5302	43.07	-22.89	20.3	4.297	0.20	0.09
GN 7756	44.63	-22.42	7.5	1.875	0.30	—
GN 7904	42.35	-21.19	34.8	6.494	0.09	0.00
GN 8292	47.54	-23.84	2.8	0.595	0.53	—
GN 9126	45.95	-22.39	5.5	1.383	1.14	—
GN 10598	44.03	-22.33	14.7	3.501	0.17	0.04
GN 11103	41.29	-18.51	9.0	1.318	0.24	0.14
GN 11216	42.37	-19.28	7.8	1.458	0.20	0.11
GN 11421	44.14	-22.45	8.6	2.087	0.14	0.02
GN 12216	46.50	-24.04	6.2	1.510	0.29	—
GN 13334	44.00	-23.14	14.8	3.516	0.14	0.01
GN 14128	42.03	-19.37	6.8	1.187	0.16	0.07
GN 14229	42.14	-20.13	6.9	1.230	0.19	0.10
GN 14242	43.67	-25.68	43.5	10.021	0.48	0.36
GN 15003	39.05	-17.72	12.3	0.892	0.24	0.08
GN 15671	44.17	-21.01	5.1	1.239	0.19	0.07
GN 16895	43.65	-21.17	6.3	1.436	0.23	0.11
GN 17217	44.16	-21.09	6.8	1.649	0.62	0.50
GN 17606	38.68	-17.75	14.1	0.899	0.20	0.03
GN 19857	43.12	-19.39	4.0	0.858	0.20	0.09
GN 19996	45.10	-23.07	6.5	1.650	0.45	—
GN 21633	41.94	-19.34	9.1	1.566	0.18	0.09
GN 21983	44.32	-21.43	5.9	1.440	0.22	0.11
GN 24520	46.26	-22.52	2.7	0.671	0.61	—
GN 24667	47.45	-23.83	3.0	0.662	0.61	—
GN 25431	40.11	-18.97	20.0	2.083	0.15	0.02
GN 25594	42.33	-20.22	6.7	1.249	0.55	0.46
GN 28407	41.26	-18.91	11.5	1.668	0.12	0.02
GN 31118	46.96	-25.09	4.3	0.991	0.40	—
GS 467	44.20	-22.17	5.0	1.213	0.72	0.60
GS 895	42.23	-24.07	51.0	9.295	0.12	0.03
GS 1036	42.48	-18.86	5.3	1.010	0.24	0.15
GS 1222	38.70	-15.05	5.3	0.336	0.34	0.17
GS 3739	45.39	-23.02	4.8	1.209	0.96	—
GS 5632	44.04	-21.02	6.4	1.531	0.40	0.27
GS 6321	43.28	-21.78	13.8	3.010	0.14	0.03
GS 6587	41.74	-19.01	3.3	0.531	0.19	0.10

TABLE 2—*Continued*

ID	$m - M$	M_z	$R_{hl,z}$ (pixel)	$R_{hl,z}$ (kpc)	$\Delta(i - z)_{SSP}$	$\Delta(i - z)_{crit}$
(1)	(2)	(3)	(4)	(5)	(6)	(7)
GS 6961	42.60	-22.03	11.0	2.157	0.14	0.04
GS 7517	45.15	-21.69	2.6	0.661	0.58	—
GS 8047	43.03	-19.57	5.0	1.051	0.16	0.05
GS 9479	44.01	-20.66	4.0	0.955	0.42	0.29
GS 10754	42.24	-19.49	3.8	0.685	0.27	0.18
GS 11796	42.80	-20.56	4.0	0.812	0.23	0.13
GS 12120	40.67	-18.47	4.0	0.493	0.30	0.19
GS 13482	43.02	-21.72	8.0	1.683	0.15	0.05
GS 17085	43.99	-24.15	16.5	3.928	0.52	0.39
GS 20048	43.02	-21.16	8.6	1.800	0.16	0.06
GS 20244	45.37	-21.83	4.9	1.240	0.39	—
GS 20457	43.63	-23.20	9.3	2.119	0.51	0.39
GS 21636	42.38	-21.76	13.5	2.535	0.12	0.03
GS 22653	47.51	-25.08	4.0	0.870	0.66	—
GS 23362	43.31	-20.83	4.8	1.044	0.46	0.35
GS 24938	40.13	-16.57	4.8	0.506	0.20	0.07
GS 27149	42.63	-19.82	5.5	1.075	0.43	0.33
GS 27611	43.28	-19.58	6.3	1.379	0.32	0.21
GS 28929	41.73	-18.70	6.3	1.030	0.18	0.09

NOTE.—(1) Object ID; (2) Distance modulus; (3) Absolute magnitude in the z band (observer-frame, NOT rest-frame); (4) – (5) Half-light radius in the z band (in pixel and in kpc); (6) $(i - z)$ color difference from the expected value in the SSP model (Bruzual & Charlot 2003) with $[\text{Fe}/\text{H}] = -0.4$ and $z_F = 5$; (7) $(i - z)$ color difference from the selection criteria for BEGs (at $z < 1.2$).

TABLE 3
STRUCTURAL, X-RAY, AND SPECTRAL FEATURES OF BEGs

ID	Central color distribution	Outer color distribution	$\log L_{X-ray}$ (erg s^{-1})	Spectrum
(1)	(2)	(3)	(4)	(5)
GN 1430	symmetric deep BC	tidally distorted	43.98	—
GN 3390	little variation	tidally distorted	—	—
GN 5302	symmetric deep BC	very nearby objects	43.35	—
GN 7756	asymmetric? shallow BC	very nearby objects	42.01	—
GN 7904	little variation	very nearby objects	—	—
GN 8292	asymmetric deep BC	—	44.35	—
GN 9126	asymmetric? shallow BC	tidally distorted	42.91	—
GN 10598	off-center BC	tidally distorted	41.67	—
GN 11103	symmetric shallow BC	—	—	—
GN 11216	little variation	—	—	—
GN 11421	little variation	blue outer ring	—	—
GN 12216	little variation	—	—	—
GN 13334	symmetric deep BC	—	43.57	—
GN 14128	symmetric shallow BC	—	—	—
GN 14229	symmetric shallow BC	—	—	—
GN 14242	flat	very nearby objects	41.53	—
GN 15003	asymmetric? shallow BC	—	—	—
GN 15671	symmetric shallow BC	tidally distorted	—	—
GN 16895	off-center BC	—	—	—
GN 17217	off-center BC	—	—	—
GN 17606	little variation	—	—	—
GN 19857	asymmetric shallow BC	—	—	—
GN 19996	symmetric deep BC	red inner ring	44.42	—
GN 21633	asymmetric? shallow BC	—	—	—
GN 21983	asymmetric shallow BC	—	—	—
GN 24520	asymmetric shallow BC	—	43.53	—
GN 24667	asymmetric? deep BC	—	44.12	—
GN 25431	flat	—	—	—
GN 25594	off-center BC	—	—	—
GN 28407	multiple BC	—	—	—
GN 31118	asymmetric? deep BC	red inner ring	44.58	—
GS 467	symmetric deep BC	red inner ring	43.69	AGN
GS 895	flat	—	—	absorption
GS 1036	asymmetric? shallow BC	—	—	emission
GS 1222	asymmetric? shallow BC	—	—	absorption
GS 3739	asymmetric? deep BC	red inner ring	44.40	AGN
GS 5632	symmetric shallow BC	—	—	composite
GS 6321	little variation	—	—	absorption
GS 6587	asymmetric deep BC	red inner ring	—	absorption?

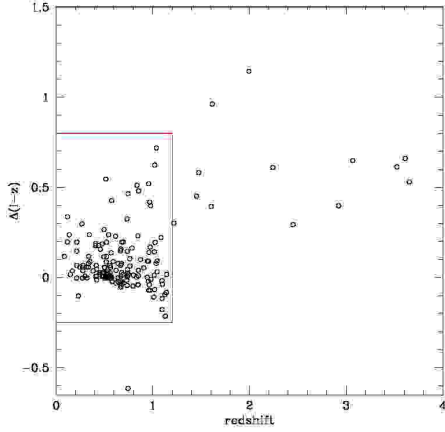


Fig. 1.— The $(i-z)_{AB}$ color differences ($\Delta(i-z) \equiv (i-z)_{\text{model}} - (i-z)_{\text{obs}}$) vs. redshift, of 171 early-type galaxies. To derive $(i-z)_{\text{model}}$, we used the SSP model (Bruzual & Charlot 2003) with $z_F = 5$ and $[\text{Fe}/\text{H}] = -0.4$. The box represents the domain used in Fig. 2.

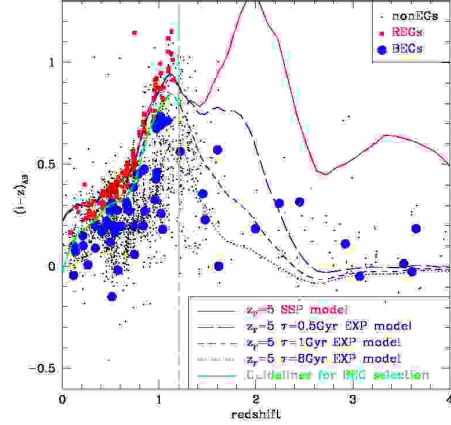


Fig. 3.— The $(i-z)$ color vs. redshift of 113 REGs (filled squares), 58 BEGs (filled circles), and 1,778 non-early-type galaxies (dots). Several evolutionary models are overlaid: SSP model with $z_F = 5$ (solid line), and exponentially-decreasing star-formation rate models (‘EXP models’) with $z_F = 5$ and $\tau = 0.5$ Gyr (long-dashed line), 1 Gyr (short-dashed line), and 8 Gyr (dotted line). We adopted $[\text{Fe}/\text{H}] = -0.4$ in all models. The dot-dashed lines are the guidelines for REG-BEG separation.

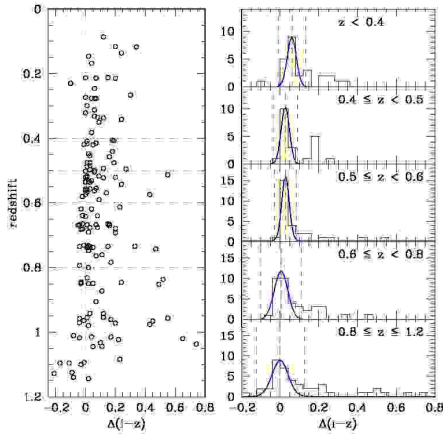


Fig. 2.— *Left panel:* The redshift vs. $\Delta(i-z)$ for $0 \leq z \leq 1.2$. We divided the redshift range into five bins so that each bin contains a similar number of galaxies (separated by four horizontal dotted lines). *Right panel:* Color histograms for five redshift bins. Curved lines represent gaussian fits. Three vertical dashed-lines represent peak- 3σ , gaussian peak, and peak+ 3σ from left to right.

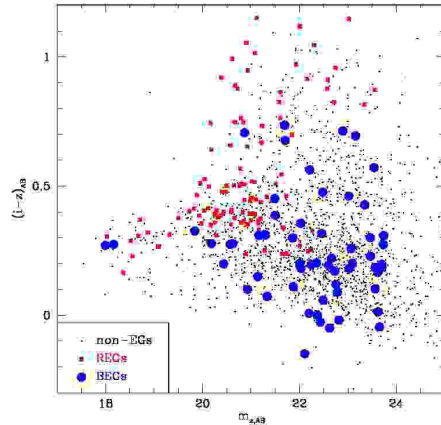


Fig. 4.— The $(i-z)_{AB}$ vs. z_{AB} of the BEGs (filled circles) in comparison with the REGs (filled squares) and non-early-type galaxies (dots).

TABLE 3—*Continued*

ID	Central color distribution	Outer color distribution	$\log L_{X-ray}$ (erg s^{-1})	Spectrum
(1)	(2)	(3)	(4)	(5)
GS 6961	symmetric shallow BC	—	43.14	AGN(+absorption?)
GS 7517	off-center BC	—	—	absorption
GS 8047	off-center BC	—	42.18	absorption
GS 9479	asymmetric shallow BC	—	—	emission?
GS 10754	symmetric deep BC	red inner ring	—	absorption
GS 11796	asymmetric deep BC	red inner ring	—	composite
GS 12120	asymmetric? deep BC	red inner ring	—	composite
GS 13482	symmetric shallow BC	—	42.35	AGN
GS 17085	flat	very nearby objects	—	absorption
GS 20048	symmetric deep BC	tidally distorted	42.93	AGN
GS 20244	asymmetric? shallow BC	—	44.38	AGN
GS 20457	symmetric deep BC	red inner ring	—	AGN
GS 21636	symmetric shallow BC	—	—	—
GS 22653	symmetric deep BC	red inner ring	44.65	AGN
GS 23362	symmetric deep BC	red inner ring	43.34	composite
GS 24938	asymmetric shallow BC	—	—	emission
GS 27149	asymmetric shallow BC	—	—	emission
GS 27611	little variation	—	—	emission
GS 28929	symmetric shallow BC	—	—	composite

NOTE.—(1) Object ID; (2) Simplified internal color distribution feature, especially about the existence of blue clumps (BCs); (3) Simplified color distribution feature, especially about tidal structures and rings; (4) X-ray luminosity in the rest-frame 0.5keV – 10keV band, calculated with a typical AGN SED; (5) Spectral line feature (CDFS only).

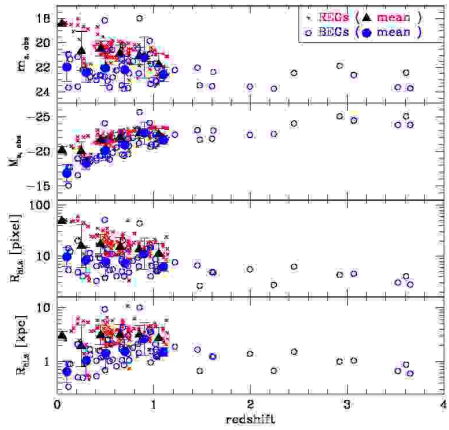


Fig. 5.— The magnitude and size distributions of the REGs (crosses) and the BEGs (open circles) as functions of redshift: apparent z -band magnitude, absolute z -band magnitude, half-light radius in pixel, and half-light radius in kpc from upper to lower. The mean values are also presented (filled triangles for the REGs and filled circles for the BEGs). The magnitudes are *not* k-corrected, because the SED of the BEGs is not well known.

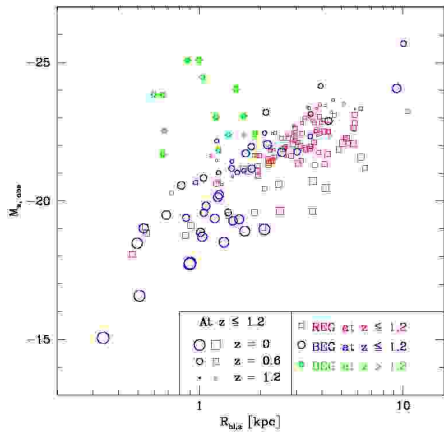


Fig. 6.— The absolute magnitude vs. the half-light radius [kpc] of the REGs (open squares) and the BEGs (open circles and open stars). For the early-type galaxies at $z \leq 1.2$, the symbol sizes decrease as redshift increases, and the BEGs at $z > 1.2$ are denoted as open stars of constant symbol size.

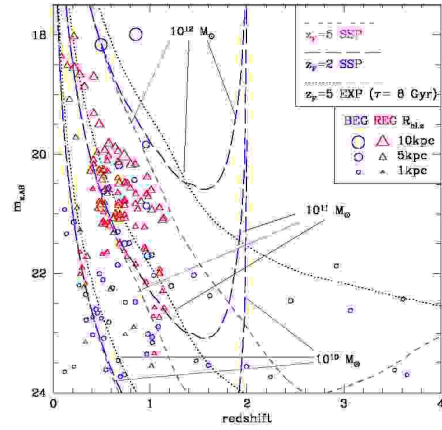


Fig. 7.— The magnitude vs. redshift of the REGs (open triangles) and the BEGs (open circles) with several galaxy evolutionary tracks from the model (Bruzual & Charlot 2003) with $[\text{Fe}/\text{H}] = -0.4$. Short-dashed lines, long-dashed lines and dotted lines represent, respectively, the SSP models of single burst at $z_F = 5$, single burst at $z_F = 2$ and exponential star-formation with $\tau = 8$ Gyr. For each model, three evolutionary lines for the masses of 10^{10} , 10^{11} , $10^{12}M_\odot$ are drawn. Symbol sizes of the BEGs and the REGs are proportional to their half-light radii.

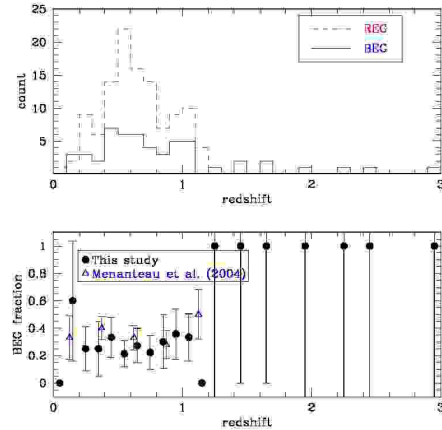


Fig. 8.— *Upper panel*: The number counts of the REGs (dashed line) and the BEGs (solid line). *Lower panel*: The variation of BEG fraction among entire early-type galaxies as a function of redshift in this study (filled circle) and in Menanteau et al. (2004) (open triangle).

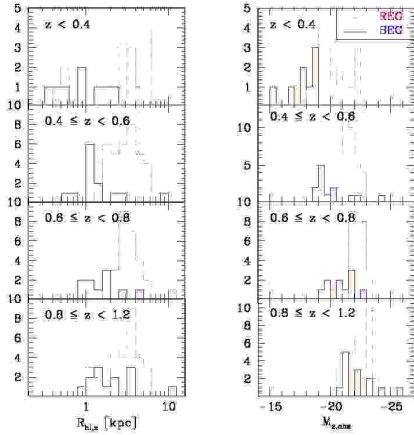


Fig. 9.— The half-light radius distribution (left panel) and the absolute magnitude distribution (right panel) of the REGs (dotted line) and the BEGs (solid line) for four redshift bins.

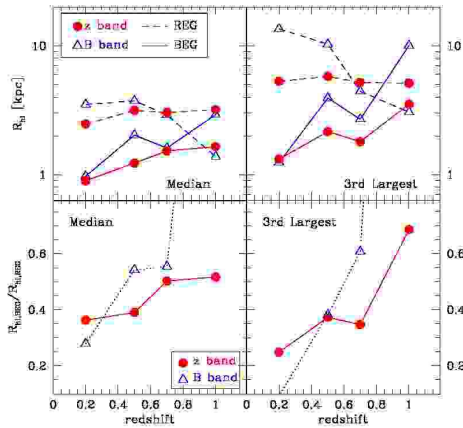


Fig. 10.— *Upper-left panel*: The median sizes of the REGs and the BEGs as functions of redshift. *Lower-left panel*: The ratio of BEG median size to REG median size as a function of redshift. *Upper-right panel*: The 3rd largest galaxy sizes of the REGs and the BEGs as functions of redshift. *Lower right panel*: The 3rd largest galaxy size ratio of BEGs to REGs as a function of redshift. Filled circles represent z band and open triangles represent B band in all panels. In the two upper panels, solid lines represent the values for the BEGs and dashed lines for the REGs.

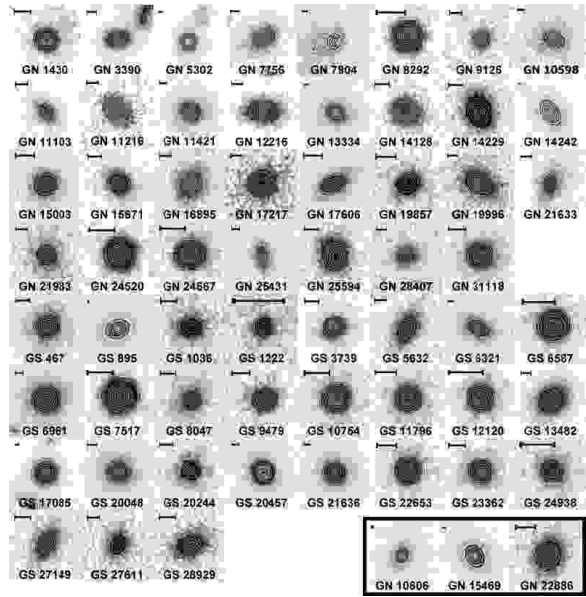


Fig. 11.— The gray-scale maps and isophotal contours of z -band images of the 58 BEGs and three typical REGs with different apparent magnitudes (GN10606, GN15469, and GN22886 at the lower-right corner; $m_z = 20.85, 18.87,$ and 22.01 respectively). The size of each image was adjusted for the best view of each galaxy based on its half-light radius, with a scale-bar indicating a physical length, 2 kpc.

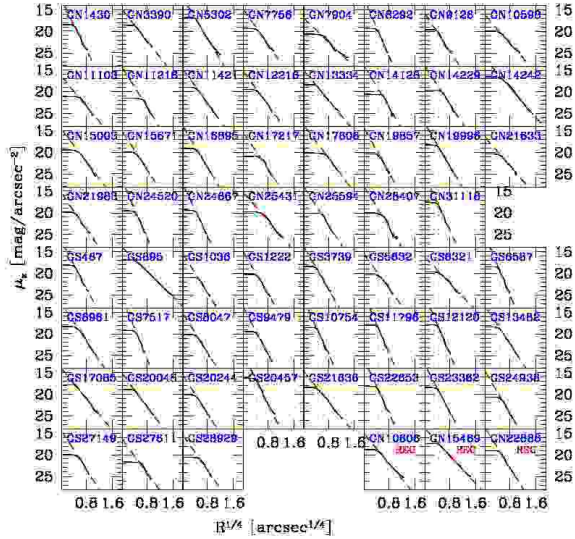


Fig. 12.— The surface brightness profiles of the 58 BEGs and three REGs for comparison in the z band. The outer part of each profile is overlaid with a $R^{1/4}$ fitting line (dashed line), and the average PSF HWHM (half width half maximum) is denoted as a vertical dotted line.

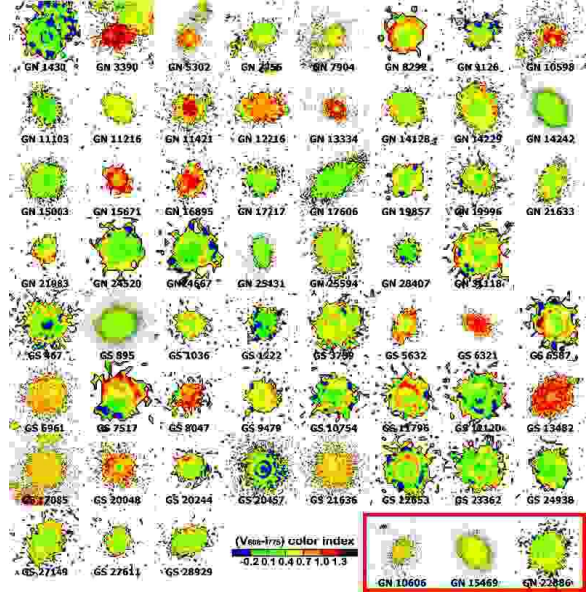


Fig. 13.— The pseudo-color maps representing the $(V - i)$ color of the BEGs, with the same sizes as the portrait images in Fig. 11. In the lower-right box, the pseudo-color images of three typical REGs are shown for comparison. The bar in the lower-center shows the $(V - i)$ range that each color tone represents.

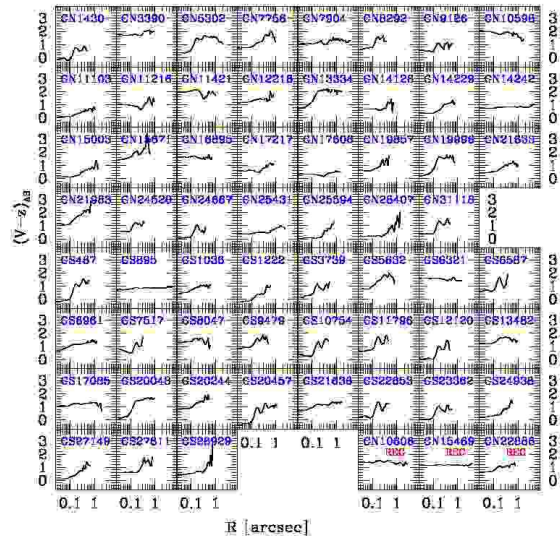


Fig. 14.— The $(V - z)$ color profiles of the 58 BEGs and three REGs. The PSF HWHM is 0.05 arcsec.

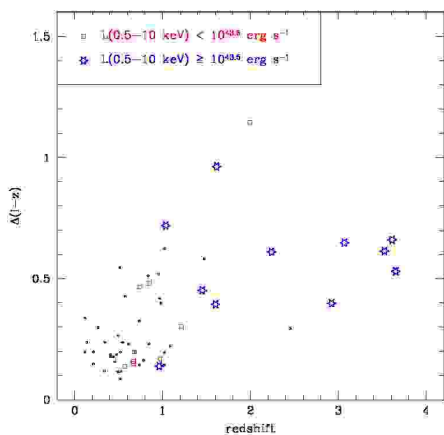


Fig. 15.— The X-ray luminosity features on the $\Delta(i-z)$ vs. redshift diagram. Open squares and open stars represent, respectively, high X-ray luminosity BEGs ($L_{0.5-10\text{keV}} \geq 10^{43.5} \text{ erg s}^{-1}$) and low X-ray luminosity BEGs ($L_{0.5-10\text{keV}} < 10^{43.5} \text{ erg s}^{-1}$). The BEGs that were not detected in the X-ray are also plotted (small open circles).

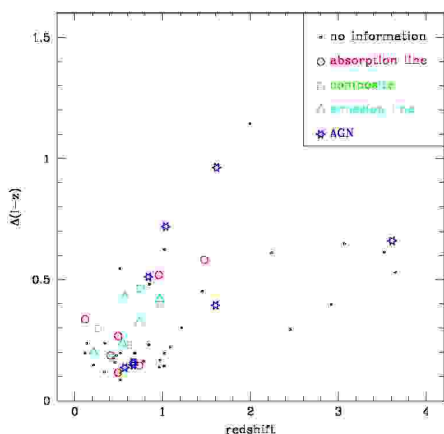


Fig. 16.— The spectral line features on the $\Delta(i-z)$ vs. redshift diagram. We classified the BEGs according to their spectral line features into four categories: absorption line galaxies (open large circles), emission line galaxies (open triangles), composite line galaxies (open squares), and AGNs (open stars). The BEGs without spectral line information (small open circles) are also plotted.

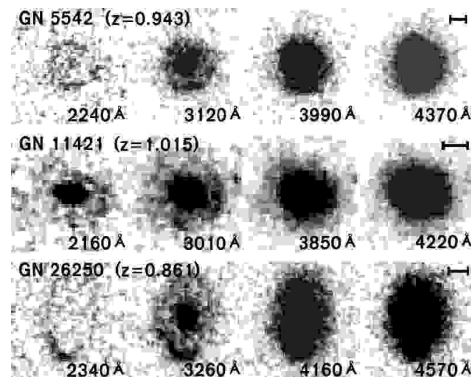


Fig. 17.— Grayscale maps of four band images of the ring galaxies. The lower-right number in each image represents the rest-frame wavelength in the B , V , i , and z bands, respectively. The scale-bar in the upper-right corner for each galaxy represents the length of 2 kpc.